- Technical Paper -

SHEAR BEHAVIOR PREDICTION OF CENTRIFUGAL FORMING HOLLOW CIRCULAR SFRC PILES USING THE FINITE ELEMENT METHOD AND X-RAY TECHNIQUE

Chi CHEN[*1], Sopokhem LIM[*2], Soichiro KONDO[*3] and Mitsuyoshi AKIYAMA[*4]

ABSTRACT

This paper presents a finite element (FE) method to assess the shear performance of hollow circular steel fiber reinforced concrete (HSFRC) piles, considering the effects of fiber distribution and orientation influenced by centrifugal forming. A novel approach is developed to identify a constitutive tensile stress-crack opening relation for the HSFRC material using prisms made of SFRC and fiber distributions observed in small HSFRC piles visualized through an X-ray technique. The FE method provides a highly accurate prediction of the shear behavior of large HSFRC piles.

Keywords: steel fiber, fiber orientation, PHC pile, centrifugal forming, X-ray, shear behavior.

1. INTRODUCTION

Steel fiber reinforced concrete (SFRC) is utilized in construction applications such as bridge decks and concrete piles. The crack-bridging forces of randomly oriented steel fibers delay the initiation and suppress the propagation of cracks, thereby improving the residual tensile strength, shear strength, and ductility of concrete structures. However, the practical application of steel fibers in concrete structures is limited due to the uncontrolled spatial distribution and orientation of fibers, which are affected by several factors during fabrication (e.g., casting method, vibration, and restricted boundary forms). A critical localized crack might occur at locations with the fewest fibers or those with poorly oriented steel fibers, leading to significantly reduced structural performance of SFRC members [1]. To address these challenges, several researchers have explored methods to manipulate the distribution and orientation of steel fibers in SFRC members (e.g., the use of magnetic fields [2] and enhancing the flowability of fresh concrete [3] to orient the steel fibers in alignment with the direction countering tensile stress).

Recently, researchers [4,5] have investigated the feasibility of replacing stirrups with steel fibers in centrifugal forming hollow circular reinforced concrete (HSFRC) piles, aiming to improve the production efficiency of hollow circular reinforced piles without the need for stirrup installation. The results of X-ray imaging showed that, under the influence of centrifugal forces, steel fibers tend to align perpendicularly to the longitudinal axis, effectively resisting shear stresses. Therefore, the inclusion of a 0.5% volume fraction of steel fibers significantly and consistently enhances the shear strength of HSFRC piles [4,5].

Regarding the prediction method for assessing the structural performance of SFRC members, most models assume a random orientation of fibers within the structure [6,7], while others consider the wall effect influencing the orientation of fibers near the boundary surfaces [8]. These simplifications are inadequate for capturing the effects of the centrifugal casting method, where most steel fibers are reoriented perpendicularly to the longitudinal axis due to centrifugal forces [4,5]. Therefore, it is necessary to develop a finite element (FE) method that considers the fiber distributions and orientations affected by centrifugal casting to predict the shear behavior of centrifugal forming HSFRC piles.

This paper develops a reliable approach to assess the shear performance of HSFRC piles using the FE method and X-ray technique, considering fiber distribution and orientation under centrifugal forces. A novel approach determines the constitutive stress-crack opening (σ-w) relation of HSFRC material using post-cracking tensile residual strengths from SFRC prisms and fiber properties from small HSFRC piles [4]. Using the σ-w relation from small specimens, the FE method predicts the shear performance of 350-mm-diameter HSFRC piles from a previous study [5]. The predicted shear behavior is validated against experimental data.

2. EXPERIEMTAL PROGERAM

2.1 Specimen details and materials

Fig.1 shows the specimen details. Six SFRC prisms, as illustrated in Fig.1(a), were made to characterize SFRC material. Fig.1(b) and Fig.1(c) depict centrifugal forming HSFRC piles with diameters of 154 mm (D154 pile) from [4] and 350 mm (D350 pile) from [5], respectively. D154 piles were used to collect data of fiber distribution and orientation under centrifugal forming conditions. The loading test results

*1 Graduate School of Creative Sciences and Engineering, Waseda University, JCI Student Member
*2 Environmental Research Institute, Waseda University
*3 Nippon Concrete Industries Co., Ltd
*4 Professor, Dept. of Civil and Environmental Engineering, Waseda University, JCI Member

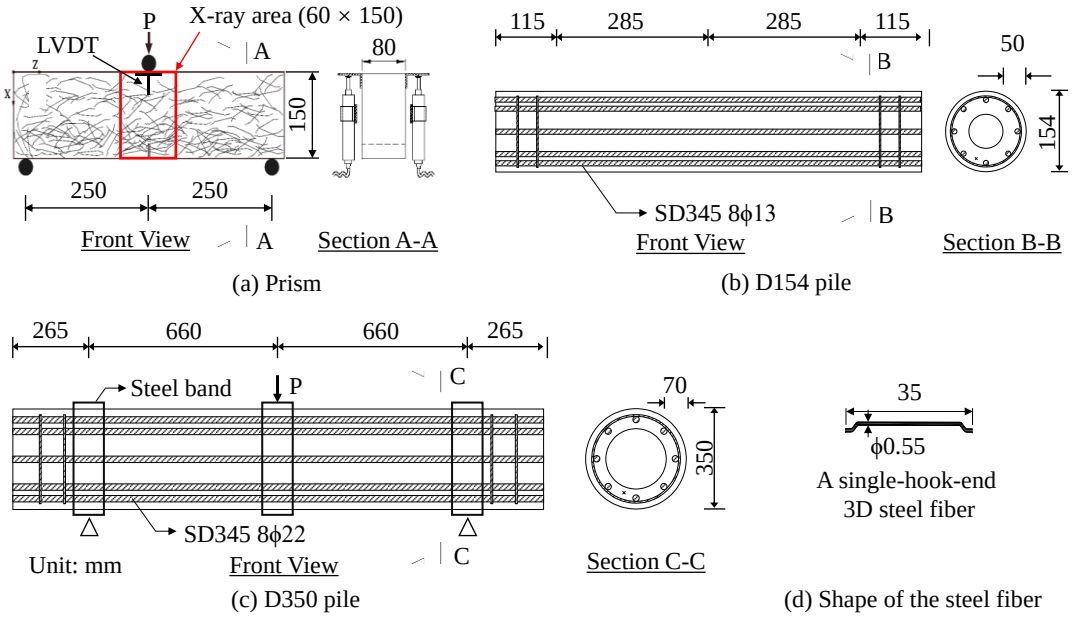

(a) Prism (b) D154 pile

(c) D350 pile (d) Shape of the steel fiber

Fig.1 Details of (a) prism, (b) D154 pile, (c) D350 pile and (d) shape of the steel fiber

of two D350 piles were compared with computational results from the FE method for validation. The prisms and D350 piles had different concrete mixtures with water-to-cement ratios of 50% and 40%, respectively. Three solid SFRC cylinders (100 mm × 200 mm) were made for compressive and splitting tensile strength tests of SFRC prisms. Three small centrifugal piles (200 mm × 300 mm) were used for the compressive strength test of D350 piles, while solid cylindrical specimens were used for splitting tensile strength tests [5]. The prismatic specimens had average compressive strength (σ'_c) and tensile strength (σ_t) of 31.6 MPa and 3.9 MPa, respectively. D350 piles had σ'_c and σ_t of 70.3 MPa and 4.4 MPa, respectively. All specimens were reinforced with 3D steel fibers at a 0.5% volume fraction. The 3D steel fiber is a single-hook-end fiber with a diameter of 0.55 mm and a length of 35 mm, as shown in Fig.1(d).

2.2 Test procedure

(1) X-ray photography

Fig.2 shows the X-ray apparatus used for imaging prisms and D154 piles. 8-bit grayscale images with a resolution of 1024 × 768 pixels were acquired. The mid-span area of the prisms imaged was 60 × 150 mm^2. An example of prism X-ray images is shown in Fig.3. Before imaging two D154 piles, they were cut into eight pieces along the longitudinal axis, and X-ray images were taken from eight angles, as shown in Fig.4. The details are provided in [4]. For D350 piles, X-ray imaging was not possible because the piles were too large for the supporting steel plate in the X-ray chamber.

(2) Loading tests

Three-point loading tests of the SFRC prisms, illustrated in Fig.1(a), were conducted to obtain the load-deflection responses of the SFRC material. The loading tests of the D350 piles, depicted in Fig.1(c), were conducted in a previous study [5] to investigate the shear behavior of centrifugal forming HSFRC piles.

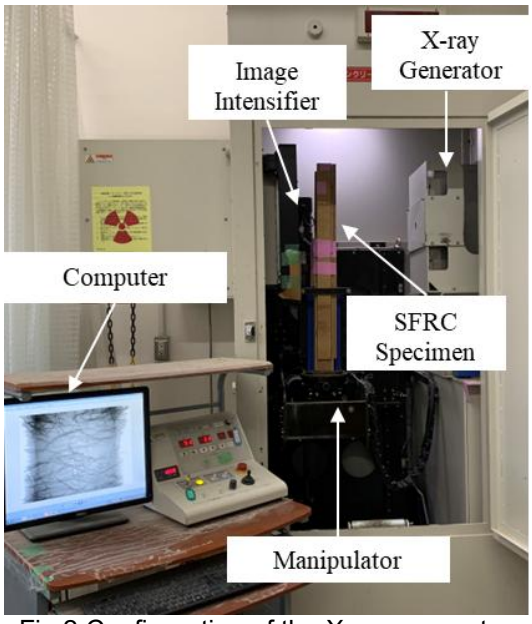

Fig.2 Configuration of the X-ray apparatus

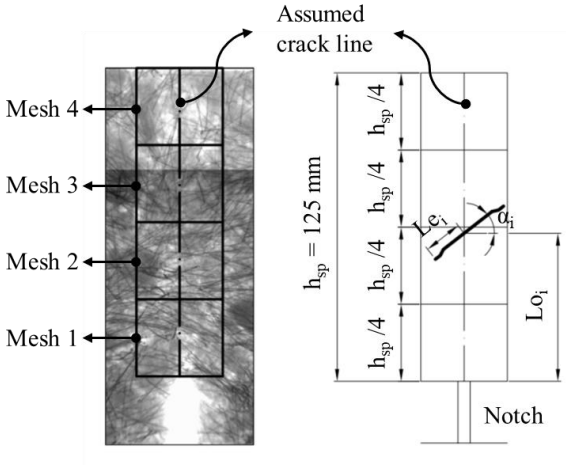

Fig.3 Measurement of fiber distribution properties in a mesh from X-ray images of SFRC prisms

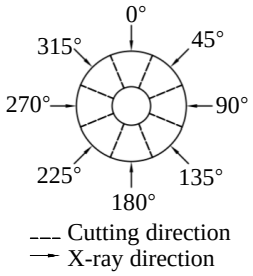

Fig.4 Cutting method of D154 pile [1]

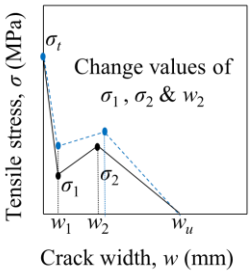

Fig.5 Trilinear tensile σ-w relation

3. IDENTIFICATION OF CONSTITUTIVE TENSILE STRESS-CRACK OPENING RELATION BASED ON THE FIBER VARIABILITY OF CENTRIFUGAL FORMING HSFRC PILES

3.1 A parameter to account for fiber variability

The post-cracking tensile residual stresses of SFRC material mainly depend on the fiber distribution and orientation at the critical section [1,9]. The dimensionless parameter RNF, which represents the orientation, embedded length, and location of double-hook-end 5D steel fibers across the assumed cracking line, was established to account for fiber variability in SFRC prisms and beams [1].

Nonetheless, there is a lack of research on the relation between the RNF of a single-hook-end 3D steel fiber and the σ-w relation of SFRC material. To establish this relation, the orientation (α) and embedded length (Le) of 3D steel fibers crossing the assumed crack line (middle line) were measured within four areas above the notch of prisms, as shown in Fig.3. The RNF of 3D steel fibers in prisms was obtained from X-ray imaging. According to [1], RNF of 3D steel fibers is calculated as:

$$\mathrm{RNF} = \sum_{i=1}^{n} \mathrm{RNF}_i = \sum_{i=1}^{n} SLe_i \times S\alpha_i \qquad (1)$$

where,

i : i^{th} fiber that crosses the assumed crack line

n : total number of fibers that cross the assumed crack line

$S\alpha_i$: score of the orientation of the i^{th} fiber

SLe_i : score of the embedded length of the i^{th} fiber

In Eq. 1, when Le_i is smaller than 5 mm which is the hook length of 3D steel fiber, SLe_i is 0.1; otherwise, SLe_i should take a value of 1.0. $S\alpha_i$ is calculated as $\cos(\alpha_i)$.

3.2 Calibration method to identify constitutive σ-w relation

A two-dimensional FE model based on [1] was employed to identify and calibrate the σ-w relation via Diana v10.6. The assumed straight crack line in the middle of the prism was modeled using a 4-node line interface element, while the remaining elements were represented as 8-node plane stress elements with an elastic stress-strain relation. The trilinear curve used by several researchers (e.g., [1]) was adopted herein for determining the tensile σ-w relation, as shown in Fig.5. This trilinear σ-w relation is used to characterize the tensile behavior of SFRC with an enhanced post-cracking tensile performance by crack-bridging steel fibers (including both 3D and 5D fibers). This trilinear curve is defined by four main points: the tensile strength σ_t at a crack width w = 0.0 mm; σ_1 representing the post-cracking residual tensile stress at w_1 just after an initial crack occurs and some active steel fibers at a crack section start to resist the tensile stress; σ_2 representing the post-cracking residual tensile stress at a critical crack width w_2 where steel fibers reached their crack-bridging potential by undergoing the pull-out of concrete matrix; and the last point with zero stress at w_u, calculated as 6.8 mm based on the average embedded length of steel fibers in the prisms [1].

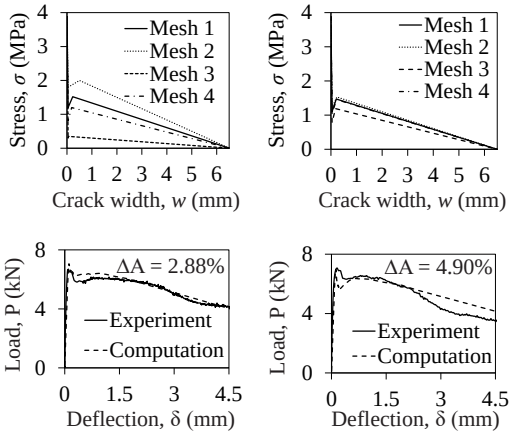

(a) prism 2 (b) prism 4

Fig.6 Trilinear σ-w relations identified from four meshes and fitted load-deflection curves of (a) prism 2 and (b) prism 4

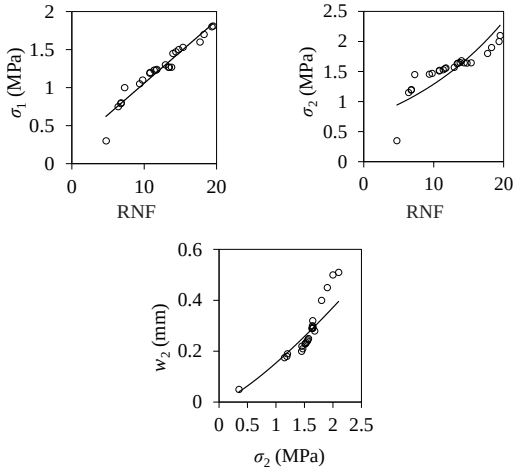

Fig.7 Relations of (a) RNF and σ_1, (b) RNF and σ_2, and (c) σ_2 and w_2

During the calibration procedure, the values of σ_1, σ_2, and w_2 were iteratively adjusted until the difference between the areas under the load-deflection curves (ΔA) obtained from experimental and computational results is less than 5% (i.e., ΔA < 5%). Just after the initial crack, the change in w_1 is insignificantly small depending

primarily on the fracture energy release rate of the concrete matrix since only a fraction of steel fibers just start to actively bridge the crack. The value of w_1 could be fixed at 0.045 mm while maintaining a good fitting of the first peak point between the computational and experimental load-deflection curves for each prism. Fig.6 illustrates the area difference in the load-deflection curves of experimental and computational results, as well as the trilinear stress-crack opening curves for prism 2 and prism 4 as examples.

3.3 Regression analysis

The variability of σ_1, σ_2, and w_2 is related to the distribution and orientation of steel fibers, which vary across SFRC specimens and can be represented by RNF. Fig.7 demonstrates that σ_1 and σ_2 exhibit a strong relationship with RNF, with $R^2 = 0.93$ and $R^2 = 0.72$, respectively; the two lowest points deviating far from the regression lines were caused by an error in estimating relationship of RNF with the lowest values of σ_1 and σ_2 due to a far deviation of the real crack from the assumed straight crack line of the prism 2 at mesh 3. Additionally, the relationship between w_2 and σ_2 is also well-described by regression analysis, showing a strong correlation with $R^2 = 0.85$. Through regression analysis, the relationships among RNF, σ_1, σ_2, and w_2 are expressed as follows:

$$\sigma_1 = 0.08\text{RNF} + 0.23 \quad (2)$$

$$\sigma_2 = 0.71\exp(0.06\text{RNF}) \quad (3)$$

$$w_2 = 0.15\sigma_2^{1.27} \quad (4)$$

3.4. RNF of centrifugal forming HSFRC piles

This study aims to establish a prediction model for a full-scale D350 pile fabricated under practical conditions at a precast concrete factory, as reported by Chen et al. [5]. However, visualizing steel fibers in a full-scale pile is challenging due to the limitations of the X-ray apparatus. Therefore, the RNF for centrifugal forming HSFRC piles is obtained from [4], which analyzes fiber distribution and orientation of D154 piles. These D154 and D350 piles have similar concrete proportions and rotation patterns and use the same type of steel fiber (3D steel fiber) with a volume fraction of 0.5%. The average RNF obtained from these D154 piles is assumed to represent the fiber distribution and orientation in the D350 piles.

An X-ray image captured from D154 piles at each angle was divided into 26 areas, each with a length of 31.25 mm, which is equal to the height of the areas above the notch of prisms, as shown in Fig.3. RNF is estimated by assuming a crack line to be parallel to the steel fibers in the vertical direction like stirrups which is assumed to be most effective against shear stresses. The steel fibers crossing the longitudinal axis were counted and converted into RNF for each area using the method described in Fig.3 and Eq. 1. The x-coordinate was corrected due to the cylindrical shape of the piles, as mentioned in [4]. Within the same mesh area, D350 with a larger thickness has a greater concrete volume and thus more steel fibers for reinforcing concrete. Even though the steel fiber distributions are similar, the RNF_{154} directly obtained from D154 was multiplied by a thickness factor in Eq. 5 before applying it to the establishment of the FE model for D350 piles. The modified RNF for D154 piles with a steel fiber volume of 0.5% is shown in Table 1.

$$\text{RNF} = \varphi\text{RNF}_{154} \quad (5)$$

where,

φ : thickness ratio of the D350 pile to the D154 pile.

Subsequently, the trilinear σ-w relation for the D350 pile can be obtained by applying the average RNF of 15.8 in Eqs. 2 to 4.

4. SHEAR PREDICTION OF CENTRIFUGAL FORMING HSFRC PILES USING FE METHOD

4.1 FE model and material constitutive stress-strain (σ-ε) relation

One pile was analyzed using the three-dimensional (3D) FE method with a rotating crack model, as shown in Fig.8, to simulate the shear behaviors of the D350 HSFRC piles from [5]. The dimensions for FE model are the same as Fig.1(c). Material properties are explained in Section 2.1. Truss elements were used for the reinforcing rebars.

Table 1 φRNF_{154} of D154 piles

	φRNF_{154}								
Pile	0°	45°	90°	135°	180°	225°	270°	315°	Average
D154-1	17.6	15.4	15.4	16.4	16.2	14.9	16.2	11.3	15.8
D154-2	14.7	18.4	16.4	15.7	17.0	17.5	15.6	14.3	

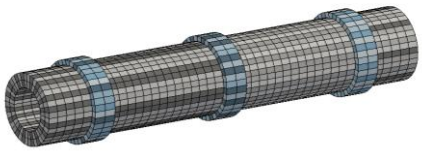

Fig.8 3D FE model for simulation of D350 piles

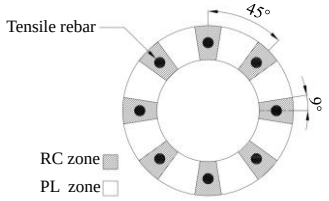

Fig.9 Specified PL and RC zones in the FE model

(1) σ-ε relation of concrete tension

According to An et al. [10], concrete located close to reinforcing rebars shows different tensile behaviors from that located far away from the reinforcing rebars. Therefore, the SFRC in the piles is divided into two zones in the simulation depending on the distance from the longitudinal rebars: a) the zone far from a rebar which only considers the effect of steel fiber reinforcement (referred to as PL zone), and b) the zone near a rebar which needs to take into account of the effect

from tension stiffening of steel bar-concrete bond effective zone and steel fibers (referred to as RC zone). To obtain RC zone with similar dimensions to the mesh in the X-ray image (i.e., average width of 31 mm), the arrangement of PL zones and RC zones are simplified based on the angles in the FE model, as shown in Fig.9.

The constitutive relations of each zone are explained below. The tensile constitutive relation of the PL zone in the HSFRC pile is illustrated as the solid black line in Fig.10. Before concrete cracking, the constitutive relation adopted by An et al. [10] is used for the PL zone:

$$\varepsilon_{cr} = 2\,\varepsilon_t = 2\,(\sigma_t / E_c) \quad (6)$$

when $\varepsilon < \varepsilon_t$,

$$\sigma = E_c\,\varepsilon \quad (7)$$

when $\varepsilon_t \le \varepsilon \le \varepsilon_{cr}$,

$$\sigma = \sigma_t \quad (8)$$

where,

σ : tensile stress
σ_t : tensile strength
ε : tensile strain
ε_t : tensile strain at the maximum tensile stress
ε_{cr} : cracking strain

The Young's modulus E_c is determined as 37,002 N/mm^2, obtained from the compression test of small centrifugal piles (200 mm × 300 mm) [2]. Following concrete cracking ε_{cr}, the trilinear stress-strain curve derived in Section 3 is utilized, as shown in Fig.10, to represent the bridging effect of steel fibers. ε_1, ε_2, and ε_u (the strain corresponding to w_1, w_2, and w_u, respectively) define the strain states after cracking:

$$\varepsilon_1 = w_1/l_{cs} + \varepsilon_{cr} \quad (9)$$

$$\varepsilon_2 = w_2/l_{cs} + \varepsilon_{cr} \quad (10)$$

$$\varepsilon_u = w_u/l_{cs} + \varepsilon_{cr} \quad (11)$$

where,

l_{cs} : characteristic length assumed to be equivalent to the outer radius of the D350 pile

The constitutive relation of the RC zone in the HSFRC pile is illustrated in Fig.10. When $\varepsilon < \varepsilon_{cr}$, the tensile constitutive relation of the RC zone is identical to Eqs. 6 to 8, which are applied to the PL zone. When $\varepsilon_{cr} \le \varepsilon \le \varepsilon_p$, the tensile constitutive relation of the RC zone considering the tension stiffening of steel bar-concrete bond is illustrated as the solid red line in Fig.10, which follows Eq. 12 [10]:

$$\sigma = \sigma_t\,(\varepsilon_{cr}/\varepsilon)^{0.4} \quad (12)$$

Here, ε_p represents the intersection point of the trilinear stress-strain curve derived from RNF and the curve obtained by Eq. 12. For $\varepsilon > \varepsilon_p$, σ is calculated using the same trilinear stress-strain curve obtained from RNF as in the PL zone.

(2) σ-ε relation of concrete in compression

The compressive strength σ'_c is determined through the average compression test of three small hollow piles. According to the standard equation [3], the fracture energy of the concrete under compression ($G_{\sigma'_c}$) is calculated by:

$$G_{\sigma'_c} = 8.8\sqrt{\sigma'_c} \quad (13)$$

(3) σ-ε relation of reinforcing rebars

Embedded rebar elements were employed to model the rebars. The modulus of elasticity was set to 2.0×10^5 N/mm^2 and was simulated using the Von Mises plasticity model. The bond-slip relation of rebar follows Model Code 2010. Since the purpose of this study is to investigate the shear behavior, strain hardening after the yielding of rebars was not taken into consideration.

4.2. Validity of FE model with experimental results

Fig.11 illustrates the cracking behavior on both front and back sides of (a) the test pile EXP-D350-1 and (b) the simulated pile FEA-D350 at the ultimate stage as determined from the experiment [5] and the FE method, respectively. Both piles demonstrated shear failure. In Fig.11(b), the cracking behavior of the piles simulated using the FE method is characterized by a few short and discrete diagonal cracks and approximately four critical cracks around the middle of the shear span, closely

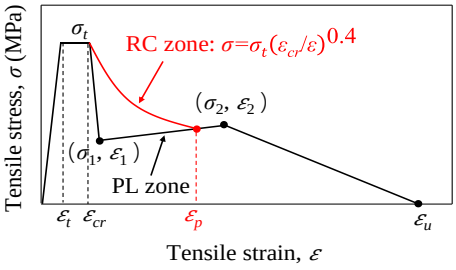

Fig.10 Tensile constitutive relation in PL zone and RC zone

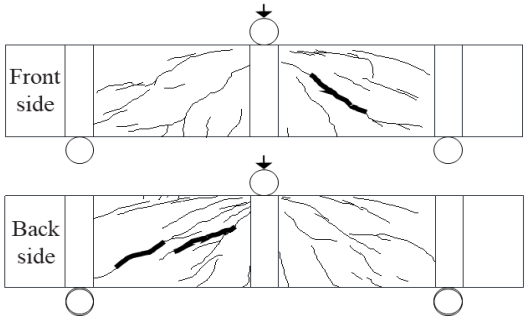

(a) Cracking behavior of the EXP-D350-1

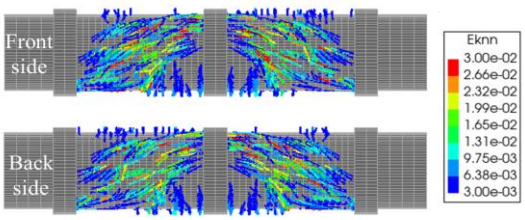

(b) Cracking behavior of the FEA-D350

Fig.11 Cracking behaviors of D350 piles

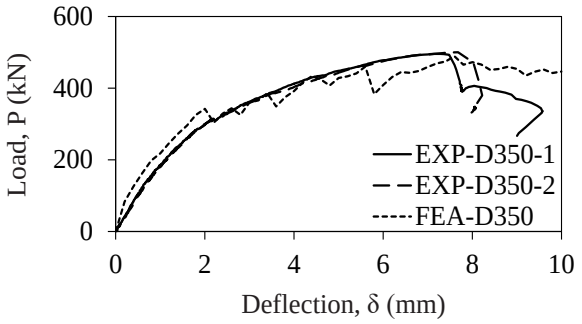

Fig.12 Load-deflection curves of D350 piles

resembling the cracking pattern of EXP-D350-1 in Fig.11(a). These results suggest that the FE model established in this study effectively simulates the crack-bridging effect of steel fibers, which suppresses crack propagation and distributes cracking more evenly.

Fig.12 illustrates the load-deflection relations of the test piles (EXP-D350-1 and EXP-D350-2) [5] and the simulated pile (FEA-D350-1). The load-deflection curve of FEA-D350 aligns well with those of EXP-D350-1 and EXP-D350-2 from the first crack to the ultimate stage. In the simulation, the first vertical crack of the simulated pile appeared at 163 kN, slightly higher than the test piles (140 kN and 120 kN). Diagonal cracks then developed at comparable loads: 273 kN, 287 kN, and 286 kN for FEA-D350, EXP-D350-1, and EXP-D350-2, respectively. All three specimens reached comparable peak loads of around 495 kN, with the FEA-D350 peak load at approximately 98% of the measured peak loads in the experiment. These results demonstrate that the proposed FE model effectively predicts the post-cracking stiffness and shear capacity of the HSFRC pile with 3D steel fibers produced by the centrifugal forming method.

5. CONCLUSIONS

This paper presents an FE model to predict the shear behavior of centrifugal forming HSFRC piles reinforced with 3D steel fibers. The model incorporates the spatial orientation of fibers influenced by centrifugal forces, as visualized using X-ray imaging. The key conclusions are as follows:

(1) The representative number of fibers (RNF) was established in this study to account for 3D steel fiber variability (i.e., distribution and orientation obtained from X-ray-derived data) in the HSFRC piles under the centrifugal forming.

(2) A novel approach was developed to determine the constitutive tensile stress-crack opening relation for HSFRC material. This method utilizes tensile residual strengths from SFRC prisms and RNF to account for fiber distribution and orientation variability in HSFRC members.

(3) The tensile trilinear stress-crack curve derived from the average RNF of D154 piles was incorporated into the 3D FE model to predict the shear behavior of D350 piles. The proposed model accurately simulated the shear behavior of 350-mm-diameter HSFRC piles, demonstrating its potential for full-scale structural assessments.

ACKNOWLEDGEMENT

The authors express sincere appreciation to Bekaert Japan Co., Ltd. for their kind support for experiments.

REFERENCES

[1] Lim S., Raju R.A., Matsuda M., Okamoto T., Akiyama M., “Structural behavior prediction of SFRC beams by a novel integrated approach of X-ray imaging and finite element method,” Construction and Building Materials, Vol.170, pp.347–365, 2018.

[2] Da Silva Brito I., Alan Strauss Rambo D., Martini S., Pícolo Salvador R., Fabrízio de Menezes Freitas M., “Flexural behavior of HPFRCC: Enhancing post-crack strength and toughness by magnetic alignment of the reinforcement,” Construction and Building Materials, Vol.269, pp.121265, 2021.

[3] Raju R.A., Lim S., Akiyama M., and Kageyama T., “Effects of concrete flow on the distribution and orientation of fibers and flexural behavior of steel fiber-reinforced self-compacting concrete beams,” Construction and Building Materials, Vol.262, pp.119963, 2020.

[4] Raju R.A., Akiyama M., Lim S., Kakegawa T., Hosono Y., “A novel casting procedure for SFRC piles without shear reinforcement using the centrifugal forming technique to manipulate the fiber orientation and distribution, ” Construction and Building Materials, Vol.303, pp.124232, 2021.

[5] Chen C., Akiyama M., Lim S., Kondo S., Hosono Y., Lai Y., Aoki K., “Shear performance of centrifugal forming hollow circular SFRC piles: Feasibility study of replacing stirrups with steel fibers,” Construction and Building Materials, Vol.409, pp.134140, 2023.

[6] Narayanan R., Darwish I.Y.S., “Use of steel fibers as shear reinforcement,” ACI Structural Journal, Vol.84, pp.216–227, 1987.

[7] Wahba K., Marzouk H., Dawood N., “Structural behavior of UHPFRC beams without stirrups,” in: Proceedings of the Canadian Society for Civil Engineering Annual Conference, pp.2487–2496, 2012

[8] Bitencourt L.A.G., Manzoli O.L., Bittencourt T.N., Vecchio F.J., “Numerical modeling of steel fiber reinforced concrete with a discrete and explicit representation of steel fibers,” International Journal of Solids and Structures, Vol.159, pp.171–190, 2019.

[9] Barros J.A.O., Cunha V.M.C.F., Ribeiro A.F., Antunes J.A.B., “Post-cracking behaviour of steel fibre reinforced concrete,” Materials and Structures, Vol.38, pp.47–56, 2005.

[10] An X., Maekawa K., Okamura H., “Numerical simulation of size effect in shear strength of RC beams,” Japanese Journal of JSCE, Vol.564, pp.297–316, 1997.

[11] Nakamura H., Higai T., “Compressive fracture energy and fracture zone length of concrete,” Modeling of Inelastic Behavior of RC Structures Under Seismic Loads, pp.471–487, 2001.